Reaction pathways and excited states in H2O2+OH→HO2+H2O: A new ab initio investigation

Bojana Ginovska, Donald M. Camaioni, and Michel Dupuis

Citation: J. Chem. Phys. **127**, 084309 (2007); doi: 10.1063/1.2755765
View online: http://dx.doi.org/10.1063/1.2755765
View Table of Contents: http://jcp.aip.org/resource/1/JCPSA6/v127/i8
Published by the AIP Publishing LLC.

Reaction pathways and excited states in $H_2O_2+OH \rightarrow HO_2+H_2O$: A new *ab initio* investigation

Bojana Ginovska
School of Electrical Engineering and Computer Science, Washington State University Tri-Cities, Richland, Washington 99354

Donald M. Camaioni and Michel Dupuis
Chemical and Material Science Division, Pacific Northwest National Laboratory, Richland, Washington 99352

(Received 9 April 2007; accepted 12 June 2007; published online 24 August 2007; publisher error corrected 27 August 2007)

The mechanism of the hydrogen abstraction reaction $H_2O_2+OH \rightarrow HO_2+H_2O$ in gas phase was revisited using density functional theory and other highly correlated wave function theories. We located two pathways for the reaction, both going through the same intermediate complex $OH-H_2O_2$, but via two distinct transition state structures that differ by the orientation of the hydroxyl hydrogen relative to the incipient hydroperoxy hydrogen. The first two excited states were calculated for selected points on the pathways. An avoided crossing between the two excited states was found on the product side of the barrier to H transfer on the ground state surface, near the transition states. We report on the calculation of the rate of the reaction in the gas phase for temperatures in the range of 250–500 K. The findings suggest that the strong temperature dependence of the rate at high temperatures is due to reaction on the low-lying excited state surface over a barrier that is much larger than on the ground state surface. © *2007 American Institute of Physics*. [DOI: 10.1063/1.2755765]

I. INTRODUCTION

Hydroxyl radical (OH·) is an important reactive species in varied chemical environments. In atmospheric chemistry it plays an important role as a catalyst in the destruction of O_3 in the stratosphere.[1] Thus the reactions leading to loss and production of OH· are considered among the most important ones in atmospheric chemistry. The reactivity of OH radicals is also relevant to several technologies, such as nuclear technology, medical technologies, and electron-driven processes in water.[2] Indeed OH is a very reactive species that results from exposure of water to radiation.[2,3] We note that an important source of OH radical is the hydrogen peroxide molecule H_2O_2 when it is subjected to photoexcitation. We note also that whenever H_2O_2 is used to generate OH radicals, for example, in advance oxidation technologies,[4,5] the reaction (1) of OH with H_2O_2 occurs in competition with other reactions that consume OH.

$$H_2O_2 + OH \rightarrow HO_2 + H_2O. \quad (1)$$

In water radiolysis, for example, H_2O_2 is produced via recombination of OH radicals in spurs.[6,7] However, the concentration does not build up significantly due in part to reaction (1).[3] Finally, in biochemistry there is considerable recent interest in the chemistry of H_2O_2 and its derivatives, in part due to their involvement in various biological processes. In fact, H_2O_2 is often used to inactivate cells and microorganisms.[8] There is growing evidence that H_2O_2 plays a role in regulating cellular functions, as well.[9]

Several computational studies have been published dealing with the reaction of OH radical with hydrogen peroxide.[10–12] The reaction is a simple hydrogen abstraction that leads to the formation of a peroxy radical and water. The unpaired electron of the OH radical recouples with the paired electrons of the proximal –OH bond in peroxide to induce the hydrogen atom transfer. The OH bond in H_2O_2 is weaker than the OH bond in H_2O, so that the reaction is exothermic by 31 kcal/mol.[13–15] The gas phase reaction kinetics are complex. An inverted temperature dependence is observed below room temperature,[16] and above 900 K, the temperature dependence is greater than that in the range of 250–900 K.[17] Lack of pressure dependence suggests that rates are at the high pressure limit and not collision dependent. The reaction scheme is depicted below (Fig. 1). From previous work[10–12] and from analogy to the case of an OH radical interacting with a water molecule,[18] there exists a hydrogen-bonded complex in the entrance channel of this simple abstraction reaction (Fig. 1, PC). In aqueous phase the reaction is known to proceed more slowly than in the gas phase,[19] an indication that the activation barrier for the process is higher in water than in the gas phase and that aqueous solvation is stronger for the reactant than for the transition state.

While the description of solvation effects on the reaction was the motivation of our research (the results of this work will be reported in a subsequent paper), we first revisited the characterization of the gas phase reaction pathway on the ground state potential energy surface for the H abstraction reaction (1) using density functional theory and other highly correlated wave function theories.

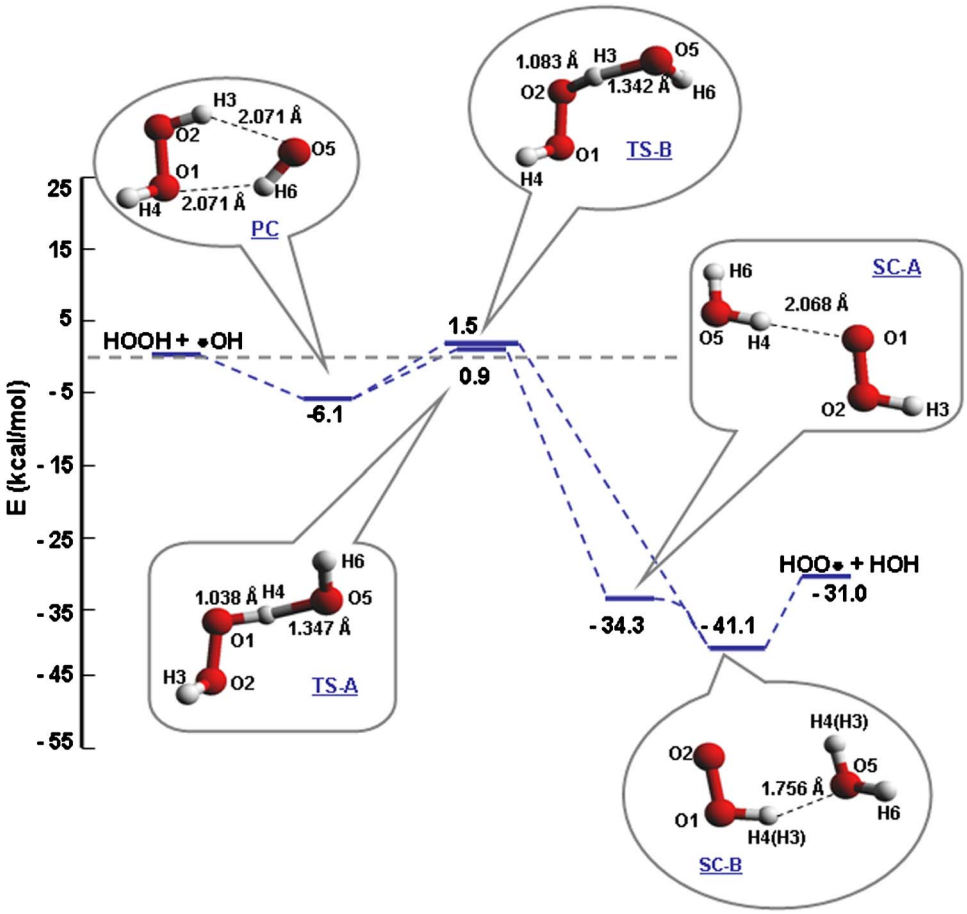

FIG. 1. (Color online) Structures of stationary points and schematic representation of the potential energy surface of the gas phase reaction HO $+H_2O_2 \rightarrow H_2O+HO_2$. The level of theory is DFT (MPW1K)/6-31+G**. The energies are not ZPE corrected (ZPE corrected energies are given in Table I).

In previous work[10–12] the structures of a precursor complex (hereinafter PC), a transition state[10,12] (hereinafter TS-A), as well as a successor complex[42] (SC-B) were identified. In this work we found a second transition state (hereinafter TS-B) over which this reaction proceeds and that involves the distal OH bond of H_2O_2. Another local minimum (SC-A) was found, higher in energy than the successor complex, which is reached following the reaction pathway from TS-A. We report here the detailed characterization of these two reaction pathways and of the potential energy surface of the ground and the first two excited states along each of these pathways. Characterization of the pathway connecting the two successor complexes SC-A and SC-B was deemed unnecessary. We report also on the calculation of the rate of the reaction in the gas phase for temperatures in the range of 250–500 K. In this range, the experimental rate measurements show Arrhenius temperature behavior with a small activation energy that is consistent with our ground state potential energy surface. Our calculations for the excited state surface show that interaction of OH with H_2O_2 splits the degeneracy of OH, giving a low-lying excited state. The resulting barrier to reaction on the excited state surface [~22 kcal/mol with time-dependent density functional theory (TDDFT) and ~32 kcal/mol with EOM-CCSD(T) levels of theory] is much higher than the barrier on the ground state surface, and, in fact, comparable to the activation energy[17] (~29 kcal/mol) for the strong temperature dependence experimentally observed above 900 K. Thus, we suggest that the high temperature reaction involves reaction on ground and excited state surfaces.

The computational methods employed for this work are presented in Sec. II. In Sec. III we present the results of the calculations and discuss our findings. The conclusions are summarized in Sec. IV.

II. COMPUTATIONAL METHODS

The geometries of the minima and the saddle points on the potential energy surface were optimized with GAUSSIAN 98 (Ref. 20) using the DFT level of theory with the 6-31+G(d,p) (6D), i.e., 6-31+G** basis set and the MPW1K hybrid density functional.[21] The minimum energy paths were calculated using the corrected local quadratic approximation Page-McIver integrator, with the program DIRDYGAUSS.[22] Ground and the two excited states calculations were carried out for points along the minimum energy paths using the time-dependent DFT method with Tamm-Dancoff approximation, as well as the completely renormalized equation-of-motion coupled cluster approach with singles, doubles, and noniterative triples CR-EOM-CCSD(T) (Ref. 23) implemented in NWCHEM-5.0.[24] We also used the complete active space self-consistent-field level of theory (CASSCF) with Nakano's multiconfiguration quasidegenerate perturbation theory (MCQDPT2) correction,[25,26] implemented in HONDO-2006.[27] The H_2O_2+OH system has 18 valence orbitals, 14 of which are occupied in the Hartree-Fock wave function. The orbitals are the three 1*s* orbitals of the oxygen atoms, the three 2*s* orbitals of the oxygen atoms, the three lone pair orbitals of the oxygen atoms, four σ bonding orbitals (three OH bonding orbitals and one OO bonding orbital),

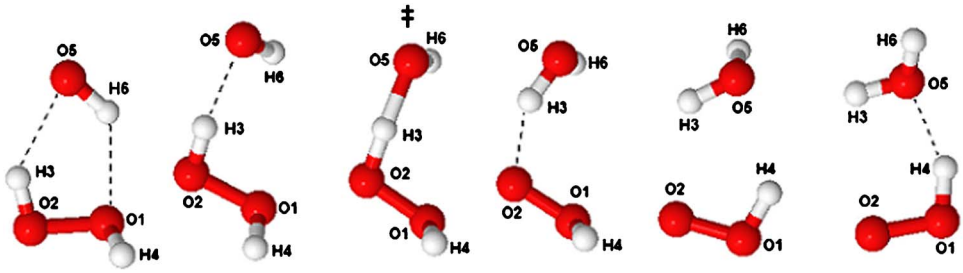

FIG. 2. (Color online) Snapshot structures along the minimum energy path for the reaction via TS-B.

and the unpaired electron orbital, along with the four σ^* antibonding OH and OO orbitals. The CASSCF wave function denoted by CAS($11e$;$10o$) was constructed by distributing 11 electrons among 10 valence orbitals [excluding the O($1s$) and O($2s$) orbitals and the two lone pairs of the oxygen atoms in H_2O_2] in all possible ways consistent with doublet spin and spatial symmetry A (no symmetry).

The dependence of the energetics on the level of theory was investigated by comparing the ground state energies of DFT(MPW1K) level of theory, with those of the partially spin restricted (RHF-RCCSD) (Ref. 28) open-shell coupled cluster theory with perturbative triples [RHF-RCCSD(T)] (Ref. 29) implemented in MOLPRO (Ref. 30) and UCCSD(T) method implemented in GAUSSIAN 98.[20] For basis set convergence calculation, Dunning's correlation consistent basis sets,[31] aug-cc-PVDZ, aug-cc-PVTZ, and aug-cc-PVQZ basis sets were used at RHF-RCCSD (T) level of theory.

The reaction rates were calculated using canonical variational transition state theory[32] with quantum effects included through the methods of zero curvature tunneling[33,34] (ZCT) and small curvature tunneling (SCT).[35,36] We corrected for hindered rotations using Truhlar's method of interpolating the partition function between the free-rotor and harmonic-oscillator limit,[37] for torsion around O–O axis in H_2O_2 and for the three low-frequency torsions in the transition states. The calculations were carried out with the program POLYRATE 9.3.1 (Ref. 38) for the temperature range of 250–500 K. The total rate was estimated as the sum of the rates for each of the reaction pathways. The energetics used in the rate calculations are those obtained with MPW1K/6-31+G** level of theory. The MPW1K geometries were used without reoptimization.

III. RESULTS AND DISCUSSION

A. The reaction pathways

In what follows we first give a brief overview of the findings and continue with a detailed analysis of the structures and pathways. The reaction of hydrogen abstraction from H_2O_2 proceeds via a PC, a five member ringlike structure, with two hydrogen bonds (Fig. 1, PC). Except for one hydrogen atom of the peroxide molecule, all the other atoms essentially reside in a plane. It is worth noting that in the precursor complex the hydrogen bond between peroxide and the oxygen atom of the OH radical involves the $2p$ lone pair of electrons of the OH radical, with the unpaired electron of the OH radical residing in the $2p$ orbital quasiperpendicular to the plane of the five member ring. This is the most energetically favorable configuration. From this precursor complex, the reaction follows one of two pathways.

The most chemically intuitive pathway involves the direct attack of the proximal –OH bond of the peroxide molecule by the oxygen atom of the OH radical. Interestingly, for the hydrogen atom transfer to occur, it must be the unpaired electron of the OH radical attacking the proximal –OH bond. This is accomplished with a change in electronic configuration of the OH radical, when one of the two electrons in the oxygen lone pair of the OH radical gets excited into the singly occupied $2p$ orbital of the same atom (in electronic structure terminology, this change in electronic structure corresponds to a single excitation). In any case, the reaction is a typical H atom abstraction reaction: the H atom transfers from peroxide to OH and, following the transition state along the pathway, the system evolves toward a successor complex where the newly formed water molecule is hydrogen bonded to the newly formed peroxy radical. This pathway is depicted in Fig. 2.

A less chemically intuitive pathway involves hydrogen atom abstraction from the distal OH bond of the peroxide molecule. It involves concerted rotations of the OH radical and of the H_2O_2 molecule, specifically a rotation of the peroxide molecule about the O–O bond in concert with the breaking of the peroxide-OH hydrogen bonds through a rotation of the OH radical. These rotations correspond to low-frequency vibrational modes of the PC complex. The oxygen atom of the OH radical ends up interacting with what used to be the distal hydrogen atom of the peroxide molecule. Following this intricate concerted atomic rearrangement, the OH radical abstracts the distal H atom on its way to a successor complex. This pathway is depicted in Fig. 3. Both pathways proceed toward successor complexes (one for each of the two pathways) where the proxy radical is hydrogen bonded to the water molecule.

The reaction may reach one of two transition state structures labeled TS-A or TS-B (Fig. 1). The two transition states have notably different structures. They differ in the orientation of the hydroxyl hydrogen and incipient hydroperoxyl hydrogen relative to the plane formed by the three oxygen atoms in the system: the hydrogen atoms are either on the same side (*cis*) (TS-A) or on the opposite side (*trans*) of the plane (TS-B). The dihedral angle that defines this orientation (O1-O2-O5-H6) is −139.8° for TS-A and 70.2° for TS-B. The bond lengths of the OH bonds being broken and being formed at the transition states are shown in Fig. 1. The structure TS-A has been previously reported[10,12] in the literature. To the best of our knowledge no mention of TS-B has been made in the literature.

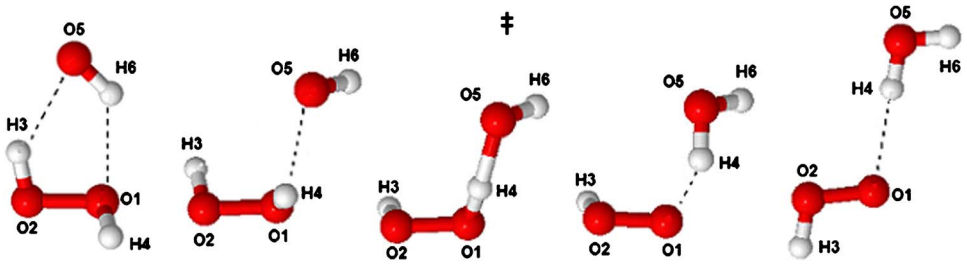

FIG. 3. (Color online) Snapshot structures along the minimum energy path for the reaction via TS-A.

The reaction paths are determined by the cleavage of the hydrogen bonds in PC. If the H3-O5 bond breaks first, as shown in Fig. 3, then the O1-H6 bond shortens and H4 exhibits electrophylic attraction to O5, so the H_2O_2 molecule rotates around the O1-O2 axis, allowing H4 to be abstracted. As the two species drift apart, the HO_2 radical continues rotating, moving H3 away from O5 and allowing O1 to form a hydrogen bond with H4 of the newly formed water molecule in a nearly planar structure (SC-A). This structure is a local minimum on the potential energy surface, about 7 kcal/mol higher in energy than SC-B. If the O1-H6 bond breaks first, as shown in Fig. 2, then the H3-O5 bond shortens and the H6 atom moves away from the plane defined by the three oxygen atoms, in the direction opposite from the H4 atom of H_2O_2. This pathway reaches the transition state TS-B. Late in the reaction, after H3 is transferred, the O5 atom of the product water molecule exhibits electrostatic attraction to the H4 atom of the product HO_2 radical, to form the hydrogen-bonded successor complex (SC-B). This pathway (Fig. 2) does not pass through SC-A.

As the reaction approaches the transition state, the OH radical changes its electronic configuration and the H abstraction occurs with the unpaired electron of the OH radical attacking one of the O–H bonds of hydrogen peroxide. In the transition state the wave function is most simply represented schematically by a complete active space wave function CAS (three electrons; three orbitals), as illustrated in Fig. 4. The three orbitals are the bonding and antibonding orbitals of the OH bond together with the unpaired electron orbital of the OH radical. The electrons are those from the OH bond and from the unpaired radical electron on OH radical. The electronic configuration mixing for the bond breaking and formation involves spatial and spin uncoupling of the OH bond electrons followed by spin recouping in the newly formed HO bond.

The energies of the species and the complex structures of the reaction, calculated with MPWIK/6-31+G** theory, are shown in Fig. 1, with the zero-point energy (ZPE) corrected values listed in Table I. The calculated exothermicity for the reaction is in good accord with experimental thermochemical energies. The basis set dependencies of the relative energies for the reactants, products, complexes, and transition states are discussed in detail below.

B. Excited states

The vertical excitation energies were calculated for the two lowest excited states for the precursor and successor complexes, for the two transition states, and also for a selected number of points along the two ground state reaction pathways. We used several theories, including TDDFT as well as the MCQDPT2 level of theory. The ground state of the OH radical in the gas phase has doubly degenerate $^2\Pi$ symmetry. In the precursor complex the degeneracy is lifted because of the interaction with the peroxide molecule, in a manner similar to what was observed in the interaction of OH with water.[18,39,40] The structure of the ground state was described above. The electronic interactions in the ground state of the precursor complex are determined by the electron occupancy in the OH radical, i.e., the "out-of-plane" $2p$ orbital is singly occupied and the "in-plane" orbital hydrogen bonded to the peroxide molecule is doubly occupied. The low-lying first excited state differs from the ground state through a single excitation involving these two orbitals. Thus, the interaction between the two components of the degenerate state remains weak and the two states (ground and low-lying excited) remain close in energy in the entrance channels of the reaction pathways.

On the reactant side, the second excited state corresponds to an electronic excitation of a σ electron of the OH bond of the hydroxyl radical into the unpaired $2p$ orbital on the O atom of the OH radical. For an isolated gas phase hydroxyl radical, the $\sigma \rightarrow \pi$ excited state is found to be ~4.2 eV above the ground state when applying the MC-QDPT2 method on the wave function averaged over the two components of the degenerate π state and the first excited state. Experimentally, this electronic transition is found to occur around 308 nm (4.0 eV).[41] In the successor complex, the first excited state corresponds to an electronic transition of an electron from the in-plane lone pair on the terminal O in HO_2 into the out-of-plane $2p$ orbital on the same terminal oxygen atom (see SC in Fig. 4). This excitation is of the same type as the low-lying excitation in the OH radical, but the excitation energy is larger in HO_2, ~1 eV. The second excited state corresponds to an electronic transition from the electron lone pair on the central oxygen atom of HO_2 to the singly occupied radical orbital of the terminal oxygen. In the

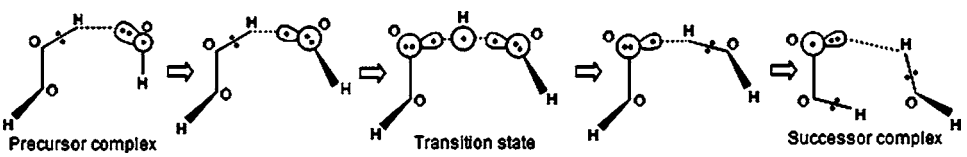

FIG. 4. Schematic of the orbitals involved in the hydrogen abstraction.

TABLE I. Energetics for the $HO+H_2O_2 \rightarrow H_2O+HO_2$ reaction from the DFT (MPW1K)/6-31+G** level of theory.

Structure	E (kcal/mol)	E+ZPE (kcal/mol)
H_2O_2+OH	0.0[a]	0.0
$OH-H_2O_2$ (PC)	−6.3	−4.4
H_3O_3 (TS -A)	0.9	0.1
H_3O_3 (TS-B)	1.5	0.2
H_2O-O_2H (SC-A)	−34.3	−32.4
H_2O-O_2H (SC-B)	−41.1	−38.3
HO_2+H_2O	−31.0	−30.7

[a]Total energy for H_2O_2+OH is −227.202 835 hartree. The ZPE correction is 23.1 kcal/mol.

precursor complex and in the successor complex the excitation energies are slightly larger than in the isolated species, due to the hydrogen bonding that holds the complexes together. The calculated energies are displayed in Table II. The calculated values are in semiquantitative accord with the experimental values both for the low-lying excited state and the second excited state.

C. Activation energies for the ground and low-lying excited states

The results described below are summarized in Tables II and III. The barrier heights on the ground state pathways are 7.3 (TS-A) and 7.8 kcal/mol (TS-B) above the precursor complex. The precursor complex is 6.2 kcal/mol lower in energy than the separated H_2O_2 and OH species. Figure 5 shows the energies of the ground state and the first two excited states calculated using TDDFT for points of the reaction pathway near the transition state TS-A The zero of energy in Fig. 5 is assigned to the PC. The potential energy surfaces for the ground and the excited states for the pathway proceeding via TS-B are very similar to those going through TS-A. An avoided crossing is visible near the transition state, between the first and the second excited state on both pathways. The barrier heights (measured from the energy of the separated reactants) on the first excited state potential surfaces are 24.6 kcal/mol for the TS-A pathway and

TABLE II. Vertical excitation energies (relative to the separated reactant species) using 6-31+G** basis set. [Energies in kcal/mol (values in parenthesis are in eV)].

	PC	TS-A	TS-B	SC-A
		EOM-CCSD(T)		
Ground state	−5.5(−0.2)	6.4(0.3)		−38.4(−1.7)
First excited state	2.0(0.1)	22.0(1.0)		−9.3(−0.4)
Second excited state	88.2(3.8)	59.5(2.6)		110.2(4.8)
		TDDFT		
Ground state	−6.2(−0.3)	1.6(0.1)	1.1(0.0)	−38.9(−1.7)
First excited state	2.4(0.1)	14.3(0.6)	18.2(0.8)	−10.4(−0.5)
Second excited state	84.5(3.7)	51.9(2.3)	57.2(2.5)	112.3(4.9)
		MCQDPT2		
Ground state	−4.2(−0.2)	7.8(0.3)	7.1(0.3)	−45.2(−2.0)
First excited state	−2.1(−0.1)	20.2(0.9)	16.5(0.7)	−16.8(−0.7)
Second excited state				

TABLE III. Vertical excitation energies and activation energies.

	TS-A (kcal/mol)	TS-B (kcal/mol)
TDDFT		
$E_{gap}(A-^2A \rightarrow B-^2A)$	17.2[a]	13.2[a]
$E^{\ddagger}(A-^2A)$	24.6[a]	22.0[a]
EOM-CCSD(T)		
$E_{gap}(A-^2A \rightarrow B-^2A)$	14.4[a]	
$E^{\ddagger}(A-^2A)$	32.6[a]	

[a]Barriers are displaced from the transition state towards the products. $E_{gap}(A-^2A \rightarrow B-^2A)$ is the energy difference between the first and second excited state the avoided crossing region, $E^{\ddagger}(A-^2A)$ is the activation energy for the first excited state (measured from the separated reactants).

22.0 kcal/mol for the TS-B pathway. The barriers are slightly displaced towards the product region compared to the ground state barriers and are significantly narrower. The separation between the two excited states in the avoided-crossing region is about 17.2 kcal/mol (0.7 eV) for TS-A and 13.2 kcal/mol (0.6 eV) for TS-B. The TDDFT calculations show that in the precursor complex, the first excited state is 0.3 eV above the ground state, and the second excited state is 3.9 eV above the ground state. The respective excited states for the successor complex (SC-B) are 1.2 and 6.5 eV above the ground state. The results are in good agreement with the results reported by Aloisio *et al.*[42] for the same structure optimized at B3LYP/6-311++G(3df,3pd) level of theory, obtained by CASSCF and MRCI. The calculated excited state energies for the PC are consistent with the values reported by Du *et al.*[18] for the H_2O-OH complex using the CCSD(T)/aug-cc-pVTZ level of theory. The second excited state was not reported in their study.

The EOM-CCSD(T) excited state calculations and the TDDFT calculations are in near quantitative accord. The

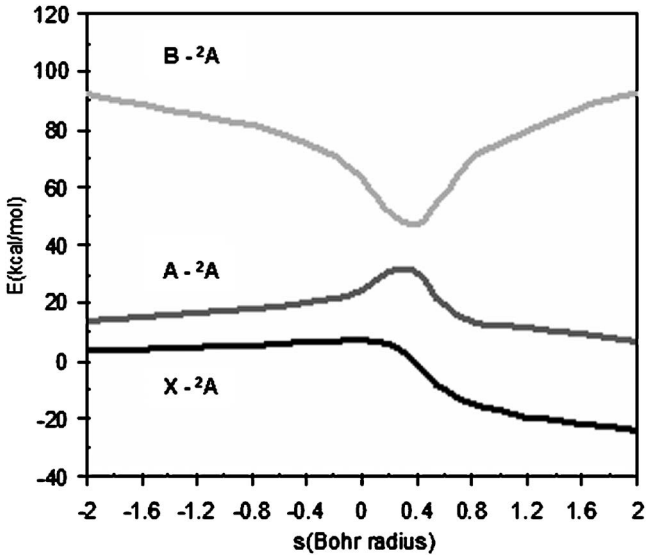

FIG. 5. TDDFT potential energy for the ground and first and second excited states near TS-A. The energies are calculated at DFT(MPW1K)/6-31+G** ground state geometries along the IRC path. In this section of the path the IRC coordinate is mainly the O1-H4 bond length. PC is assigned zero energy.

TABLE IV. $X-^2A$ energetics dependence on the basis set at DFT (MPW1K/6-31+G**) level of theory.

	DFT (MPW1K) (kcal/mol)			RHF-CCSD(T) (kcal/mol)		
Structures	aug-cc-pVDZ	aug-cc-pVTZ	aug-cc-pVQZ	aug-cc-pVDZ	aug-cc-pVTZ	aug-cc-pVQZ
H_2O_2+OH	0.0	0.0	0.0	0.0	0.0	0.0
OH-H_2O_2 (PC)	−5.7	−5.2	−4.3	−3.8	−3.7	−3.5
H_3O_3 (TS-A)	1.1	2.6	3.2	4.9	4.7	4.9
H_3O_3 (TS-B)	1.6	2.2	2.6	5.5	5.5	5.7
H_2O-O_2H (SC-A)	−34.6	−34.4	−34.1	−33.9	−34.3	−34.7
H_2O-O_2H (SC-B)	−40.4	−39.9	−39.6	−39.5	−40.1	−40.6
HO_2+H_2O	−31.7	−31.5	−31.7	−30.2	−30.8	−31.4

CCSD(T) ground state barrier for TS-A is about 4.6 kcal/mol higher than the TDDFT barrier. Due to instability of the EOM-CCSD(T) calculation, a reliable result for TS-B could not be obtained. The first and the second excited states are 0.3 and 4.1 eV above the ground state in the precursor complex. For the successor complex these energies are 1.3 and 6.6 eV. The vertical excitation at TS-A for the first excited state is 15.6 kcal/mol (0.7 eV), and is about 1.5 kcal/mol lower than the excitation energy obtained with TDDFT. For the second excited state, the vertical excitation of 53.1 kcal/mol (2.3 eV) is about 3.0 kcal/mol lower than the TDDFT value. The barrier height of the first excited state is 32.6 kcal/mol, and the energy difference between the two states in the avoided crossing region is 14.4 kcal/mol. Overall the EOM-CCSD(T) and TDDFT results are in good accord and give confidence about the accuracy of the TDDFT results.

We also performed CASSCF/MCQDPT2 calculations using orbitals averaged over the ground and the first excited state. This was necessary to facilitate the calculation of the reference CAS wave function. The transition states were found to be 7.8 and 7.1 kcal/mol above the separated reactant species for TS-A and TS-B, respectively. At the MC-QDPT2 level of theory the first excited state is calculated to be 0.1 eV above the ground state for the precursor complex and 1.2 eV for the successor complex. In general the three theories yield the same near quantitative pictures of the H_2O_2+OH system in its ground state and excited states.

D. Basis set effects

The results are summarized in Table IV. To verify the accuracy of the MPW1K/6-31+G** results, we carried out a set of energy calculations using the 6-31+G** basis set and Dunning's correlation consistent basis sets[31] at the MPW1K and CCSD(T) levels of theory. For all the calculations, the geometries of the extrema structures optimized with MPW1K/6-31+G** were used. Table V shows the effect of the level of theory for the calculations with the 6-31+G** basis set. Whereas the MPW1K level of theory predicts lower barriers, the partially spin restricted (RHF-RCCSD) (Ref. 28) open-shell coupled cluster theory with perturbative triples[29] implemented in MOLPRO (Ref. 30) predicts higher barriers compared to UCCSD(T) method implemented in GAUSSIAN 98.[20] The basis set dependence was investigated with Dunning's aug-cc-PVDZ, aug-cc-PVTZ, and aug-cc-PVQZ, for MPW1K and RHF-RCCSD(T). In the case of the MPW1K functional, the bigger basis sets yield higher transition state barriers and shallower wells for the precursor complex with respect to the separated species. In the RHF-RCCSD(T) calculation, there seems to be little basis set dependence in the calculated energies. For CCSD(T)/6-31G**||CCSD(T)/6-31G** level of theory, Atadinç *et al.*[12] report a barrier of 3.5 kcal/mol, which compares well to the barrier of 3.9 kcal/mol that we calculated using UCCSD(T)/6-31+G**||MPW1K/6-31+G**. These results indicate that the true barriers would lie somewhere between the RHF-RCCSD(T)/aug-cc-PVQZ||MPW1K/6-31+G** and DFT(MPW1K)/aug-cc-PVQZ||MPW1K/6-31+G** values.

E. Reaction rate calculations

There have been a number of studies, both experimental and theoretical, investigating the rate constant of the reaction (1) in the gas phase. The experimental results show the rate to vary anywhere from 8.4×10^{-13} to 2.0×10^{-12} cm^3 molecule^{-1} s^{-1} for room temperature.[43] Theoretical calculations done by Atadinç *et al.*[12] with conventional transition state theory (TST) and Eckart tunneling correction estimate the rate to be between 2.6×10^{-13} and 4.2×10^{-13} cm^3 molecule^{-1} s^{-1}, depending on the level of theory used.

In this work we used canonical variational transition

TABLE V. $X-^2A$ energetics dependence on level of theory using the 6-31+G** basis set.

Structures	RCCSD(T) (kcal/mol)	UCCSD(T) (kcal/mol)	DFT (MPW1K) (kcal/mol)
H_2O_2+OH	0.0	0.0	0.0
OH-H_2O_2 (PC)	−6.4	−6.4	−6.3
H_3O_3 (TS-A)	6.1	3.9	0.9
H_3O_3 (TS-B)	10.0	5.9	1.5
H_2O-O_2H (SC-A)	−32.9	−33.3	−34.3
H_2O-O_2H (SC-B)	−39.3	−39.7	−41.1
HO_2+H_2O	−29.4	−29.7	−31.0

TABLE VI. Rates, quantum corrections, Arrhenius activation energies, and pre-exponential factor for the two reaction pathways.

	$\kappa^{CVT/SAG}$		$k \times 10^{-13a}$ (cm^3 $molecule^{-1}$ s^{-1})		$k \times 10^{-13}$ (cm^3 $molecule^{-1}$ s^{-1})		E_a (kcal/mol)		log(A)	
T (K)	A	B	A	B	A	B	A	B	A	B
250	2.03	2.34	2.8	2.9	1.7	6.3	0.84	1.41	−12.03	−10.96
298	1.67	1.85	3.2	3.5	2.1	7.7	0.98	1.54	−11.96	−10.98
400	1.35	1.42	4.4	5.1	3.1	11.9	1.33	1.89	−11.79	−10.89
500	1.21	1.26	6.0	7.1	4.3	17.4	1.73	2.29	−11.61	−10.76

[a]Rates with SCT but without hindered rotation correction.

state theory (CVT), which corrects for the rate overestimation of TST, by varying the dividing surface between reactant and product to minimize the rate constant.

$$k^{CVT/SAG}(T,s) = \kappa^{CVT/SAG}\sigma\frac{K_bT}{h}\frac{Q^{GT}[T,s^{CVT}(T)]}{\Phi^R(T)}e^{[V_{MEP}[s^{CVT}(T)]/K_bT]}. \quad (2)$$

In the rate expression above, σ is the symmetry factor accounting for the two possibilities of hydrogen abstraction reaction from H_2O_2, K_b is Boltzmann's constant, h is Planck's constant, T is the temperature, $Q(T,s)$ is the transition state partition function and $\Phi^R(T)$ is the reactant's partition functions per unit of volume, s^{CVT} is the optimum classical position of the dividing surface, and $V_{MEP}(s)$ is the potential evaluated on the MEP. To account for quantum effects, we included zero curvature (ZCT) or small curvature (SCT) tunneling correction, through the coefficient $\kappa^{CVT/SAG}$.

Equation (2) is valid for reaction (1) provided that PC is in rapid equilibrium with the OH and H_2O_2.[2,44] The formation of PC from OH and H_2O_2 at 1 atm pressure is unfavorable for temperatures above 250 K (ΔG° increases from 1.1 kcal/mol at 250 K to 7.2 kcal/mol at 500 K). Therefore, rate constants calculated using Eq. (2) should be comparable to experiment provided conversion of PC to SC is rate limiting under experimental conditions. Since the rate constants deviate from normal Arrhenius behavior at low and high temperatures (see below), we use Eq. (2) to calculate rate constants within the range of 250–500 K.

The reaction barriers used in the calculations and the potential energy surface information along the reaction coordinate are those obtained at the MPW1K/6-31+G** level of theory. The rate constants were calculated separately for each of the reaction paths, k_A and k_B, and the total rate is the sum of k_A and k_B. The dependence of the rate on the hindered internal rotations treatment of the low-frequency torsional modes was investigated using Truhlar's method of interpolating the partition function between the free-rotor and harmonic-oscillator limit.[37] The results showed that by using the RW scheme[37] for this correction, the rate is larger by about a factor of 5. The zero curvature tunneling formulation gives slightly smaller rates than the small curvature tunneling formulation. For temperature of 298 K, the CVT rate is 4.0×10^{-13} cm^3 $molecule^{-1}$ s^{-1}, over four times slower than the TST rate, which is 1.7×10^{-12} cm^3 $molecule^{-1}$ s^{-1}. The inclusion of the small curvature tunneling treatment increases this value to 6.7×10^{-13} cm^3 $molecule^{-1}$ s^{-1}. The hindered rotation treatment makes the rate 9.8×10^{-13} cm^3 $molecule^{-1}$ s^{-1}. Rates, corrected variationally, with small curvature tunneling quantum correction and consideration of the internal hindered rotation, are given in Table VI for temperatures in the range of 250–500 K for paths A and B described above (Figs. 1–3). Also, we include the corresponding Arrhenius activation parameters for the two pathways. Path B is the faster of the two reaction paths, despite having the higher barrier. We analyzed the factors that contribute to the rates to find that factors which depend on quantum and hindered rotation corrections are larger for path B than the corresponding corrections for path A (Table VI).

The total rates are plotted in Fig. 6 along with experimental data taken from the NIST database.[43] The experimental data cluster into two groups with the preferred data being

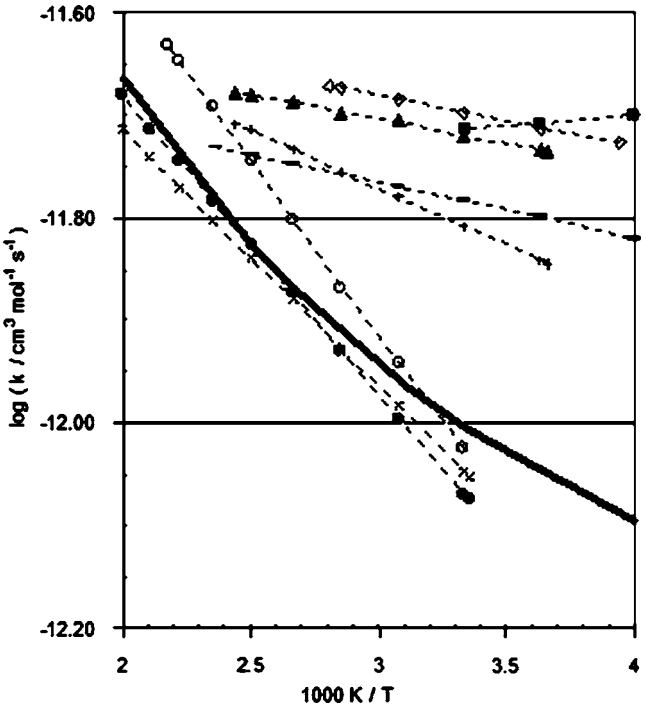

FIG. 6. Rate constants for the gas phase reaction $HO+H_2O_2 \rightarrow H_2O+HO_2$. Experiments: (◇) Ref. 47, (■) Ref. 48, (▲) Ref. 49, (+) Ref. 1, (−) Ref. 50, (×) Ref. 51, (●) Ref. 52, and (○) Ref. 53. Full line: from this work, CVT rate with RW hindered rotor treatment and small curvature tunneling correction (see text for details).

the group that exhibits higher rates and lower activation barriers. Although our calculated rates agree better with the group that exhibits lower rates and higher activation barriers, the differences are not significant considering the accuracy of the MPW1K method[21] and the rigid rotor-harmonic oscillator approximation. An Arrhenius analysis of our total rates leads to activation parameters that are larger than the preferred experimental values by less than a factor of 2 in the pre-exponential factor and less than 1 kcal/mol in the activation energy. Finally, we reiterate that in our rate calculations we assume that the precursor complex is in rapid equilibrium with the reactants. Absent in this experimental condition, the measured rates would be limited in degree by the rate of association of OH and H_2O_2, in which case smaller activation barriers may be observed.

Results discussed above (Tables IV and V) showing higher potential energy barriers at the basis set limit and at CCSD(T) levels of theory strongly suggest that the barriers calculated with MPW1K/6-31+G** are underestimated, such that the rates calculated in Fig. 6 are overestimated. One expects that with higher barriers and more accurate treatment, such as large-curvature tunneling,[32] there will be greater curvature and larger tunneling corrections that would partly compensate. In this context, we point out that Atadinç *et al.*[12] report a barrier of 3.5 kcal/mol and imaginary frequency of 2115 cm^{-1} for CCSD(T)/6-31G** level of theory. We calculated barriers of 0.9 kcal/mol at imaginary frequency of 1368 cm^{-1} (TS-B) and 1.5 kcal/mol at imaginary frequency of 1284 cm^{-1} (TS-A) at MPW1K/6-31+G**.

Measurements of the rate at lower temperatures[16] show that there is an inversion of the rate dependence below room temperature, which has been attributed to the existence of the precursor complex during the reaction.[16,45] A kinetic analysis that takes into account the pressure-dependent association and dissociation rate constants of the precursor complex[46] and tunneling along the path from PC to products should be applied to capture the non-Arrhenius behavior at low temperatures.

Unusual behavior of reaction (1) has also been observed at high temperatures. Hippler *et al.*[17] found that the rate of reaction increases greatly with T in the range of 800 K$<T\leqslant$1600 K. It corresponds to an Arrhenius activation energy of ~30 kcal/mol.[17] To account for this behavior, Hippler *et al.*[17] and later Vakhtin *et al.*[16] suggested a change in mechanism from complex formation in the lower T range to direct H transfer above 800 K. Whereas, Bahri *et al.*[10] have rationalized this behavior by suggesting that at high T the reaction occurs from the complex, whereas at lower T, collisions that form the TS directly without going into the complex are productive. The latter explanation does not seem consistent with transition state theory. At 300 K, the PC is not favored relative to the separated reactants (ΔG°=2.4 kcal/mol). Higher temperatures will have the effect of making it increasingly less stable (ΔG°=7.2 kcal/mol at 500 K). Therefore, the change in T dependence must be due to an alternative reaction path with a much higher barrier contributing to the reaction rate. We suggest that reaction via the low-lying first excited state of the reactive complex contributes at high T. Since the degeneracy of OH is lifted by complexation with H_2O_2, half of the encounters of OH with H_2O_2 lead to the excited state surface. From Table III, the lowest excited transition states are ~22 and ~32 kcal/mol above the separated reactants according to TDDFT and EOM-CCSD(T) levels of theory, respectively. Thus, the computations described above lead to a kinetic model that better explains the experimental findings, albeit more work is needed to simulate the experimental data quantitatively.

IV. SUMMARY

We revisited theoretical calculations of the reaction (1) in the gas phase as a prelude to a study of the aqueous phase reaction (in progress). In the process, we used the DFT level of theory with the MPW1K functional developed by Lynch *et al.*[21] specifically for calculating H abstraction barriers. This functional gave barrier heights and reaction energetics in good accord with experimental data, albeit in semiquantitative agreement only with other highly correlated levels of theory. Novel findings include the identification of a second TS and reaction pathway for the reaction as well as characterization of the first two excited states along the two reaction pathways. Using VTST, we calculated rate constants for the reaction in the range of 250–500 K and those were found to be in good accord with experimental values. Finally, we suggest that the strong temperature dependence of the rate at high temperatures is due to reaction on the low-lying excited state surface over a barrier that is much larger than on the ground state surface.

ACKNOWLEDGMENTS

The authors gratefully acknowledge Dr. Karol Kowalski for his assistance in preparing the EOM-CCSD(T) calculations. This work was supported in part by the Office of Basic Energy Sciences of the Department of Energy (DOE), Chemical Sciences program [for two of the authors (B.G. and M.D.)] and in part by the U.S. Department of Energy's Office of Biological and Environmental Research, Environmental Management Science Program [for two of the authors (B.G. and D.M.C.)]. The Pacific Northwest National Laboratory is operated for DOE by Battelle Memorial Institute.

[1] P. H. Whine, D. H. Semmes, and A. R. Ravishankara, J. Chem. Phys. **75**, 4390 (1981).
[2] B. C. Garrett, D. A. Dixon, D. M. Camaioni *et al.*, Chem. Rev. (Washington, D.C.) **105**, 355 (2005).
[3] G. V. Buxton, C. L. Greenstock, W. P. Helman, and A. B. Ross, J. Phys. Chem. Ref. Data **17**, 513 (1988).
[4] W. H. Glaze, J.-W. Kang, and D. H. Chapin, Ozone: Sci. Eng. **9**, 335 (1987).
[5] *Advanced Oxidation Processes for Water and Wastewater Treatment*, edited by S. Parsons (IWA, London, 2004).
[6] C. D. Jonah, M. S. Matheson, J. R. Miller, and E. J. Hart, J. Phys. Chem. **80**, 1276 (1976).
[7] A. Hiroki, S. M. Pimblott, and J. A. LaVerne, J. Phys. Chem. A **106**, 9352 (2002).
[8] A. Delabie, S. Creve, B. Coussens, and M. T. Nguyen, J. Chem. Soc., Perkin Trans. 2 **977**, 2000.
[9] G. Nindl, Cellscience Reviews **1**, 1 (2004).
[10] M. Bahri, Y. Tarchouna, N. Jaïdane, Z. Ben Lakhdar, and J. P. Flament, J. Mol. Struct.: THEOCHEM **664**, 229 (2003).
[11] B. Wang, H. Hou, and Y. Gu, Chem. Phys. Lett. **309**, 274 (1999).
[12] F. Atadinç, H. Gunaydin, A. S. Ozen, and A. Aviyente, Int. J. Chem. Kinet. **37**(8), 502 (2005).

[13] W. W. Chase, Jr., J. Phys. Chem. Ref. Data Monogr. **9**, 1 (1998).
[14] B. Ruscic, A. F. Wagner, L. B. Harding *et al.*, J. Phys. Chem. A **106**, 2727 (2002).
[15] T. M. Ramond, S. J. Blanksby, S. Kato, V. M. Bierbaum, G. E. Davico, R. L. Schwartz, W. C. Lineberger, and G. B. Ellison, J. Phys. Chem. A **106**, 9641 (2002).
[16] A. B. Vakhtin, D. C. McCabe, A. R. Ravishankara, and S. R. Leone, J. Phys. Chem. A **107**, 10642 (2003).
[17] H. Hippler, H. Neunaber, and J. Troe, J. Chem. Phys. **103**, 3510 (1995).
[18] S. Du, J. S. Francisco, G. K. Schenter, T. D. Iordanov, B. C. Garrett, M. Dupuis, and J. Li, J. Chem. Phys. **124**, 224318 (2006).
[19] H. Christensen, K. Sehested, and H. Corfitzen, J. Phys. Chem. **86**, 1588 (1982).
[20] M. J. Frisch, G. W. Trucks, H. B. Schlegel *et al.*, GAUSSIAN 98, Revision A.7, Gaussian, Inc., Pittsburgh, PA, 1998.
[21] B. J. Lynch, P. L. Fast, M. Harris, and D. G. Truhlar, J. Phys. Chem. A **104**, 4811 (2000).
[22] Y.-Y. Chuang and D. G. Truhlar, DIRDYVTST, Department of Chemistry and Super Computer Institute, University of Minnesota; Bruce C. Garrett, Environmental Molecular Sciences Laboratory, Pacific Northwest Laboratory.
[23] K. Kowalski and P. Piecuch, J. Chem. Phys. **120**, 1715 (2004).
[24] E. J. Bylaska, W. A. de Jong, K. Kowalski *et al.*, NWCHEM, version 5.0, a computational chemistry package for parallel computers, Pacific Northwest National Laboratory, Richland, Washington 99352-0999, 2006); R. A. Kendall, E. Aprà, D. E. Bernholdt *et al.*, Comput. Phys. Commun. **128**, 260 (2000).
[25] H. Nakano, J. Chem. Phys. **99**, 7983 (1993).
[26] H. Nakano, Chem. Phys. Lett. **207**, 372 (1993).
[27] M. Dupuis, A. Marquez, and E. R. Davidson, HONDO 2000, based on HONDO 95.3, Quantum Chemistry Program Exchange (QCPE), Indiana University, Bloomington, In 47405, 2000.
[28] P. J. Knowles, C. Hampel, and H.-J. Werner, J. Chem. Phys. **99**, 5219 (1993); **112**, 3106(E) (2000).
[29] J. D. Watts, J. Gauss, and R. J. Bartlett, J. Chem. Phys. **98**, 8718 (1993).
[30] H.-J. Werner, P. J. Knowles, R. Lindh *et al.*, MOLPRO, version 2002.6, a package of *ab initio* programs, see http://www.molpro.net
[31] T. H. Dunning, Jr., J. Chem. Phys. **90**, 1007 (1989).
[32] D. G. Truhlar, A. D. Isaacson, and B. C. Garrett, in *The Theory of Chemical Reaction Dynamics*, edited by M. Baer (CRC, Boca Raton, FL, 1985), Vol. 4, pp. 65–137.
[33] D. G. Truhlar and A. Kuppermann, J. Chem. Phys. **52**, 3842 (1970); J. Am. Chem. Soc. **93**, 1840 (1971).
[34] B. C. Garrett, D. G. Truhlar, R. S. Grev, and A. W. Magnuson, J. Phys. Chem. **84**, 1730 (1980); **87**, 4554 (1983).
[35] D.-h. Lu, T. N. Truong, V. S. Melissas *et al.*, Comput. Phys. Commun. **71**, 235 (1992).
[36] Y.-P. Liu, G. C. Lynch, T. N. Truong, D. Lu, and D. G. Truhlar, J. Am. Chem. Soc. **115**, 2408 (1993).
[37] Y.-Y. Chuang and D. G. Truhlar, J. Chem. Phys. **112**, 1221 (2000); **121**, 7036(E) (2004).
[38] J. C. Corchado, Y.-Y. Chuang, P. L. Fast *et al.*, POLYRATE, version 9.3.1, University of Minnesota, Minneapolis, 2005, http://comp.chem.umn.edu/polyrate
[39] K. S. Kim, H. S. Kim, J. H. Jang, H. S. Kim, B. Mhin, Y. Xie, and H. F. Schaefer III, J. Chem. Phys. **94**, 2057 (1991).
[40] Y. Xie and H. F. Schaefer III, J. Chem. Phys. **98**, 8829 (1993).
[41] K. Minschwaner, T. Canty, and C. Burnett, J. Atmos. Terr. Phys. **65**, 335 (2003).
[42] S. Aloisio, Y. Li, and J. S. Francisco, J. Chem. Phys. **110**, 9017 (1999).
[43] NIST Chemical Kinetics Database on the Web, NIST Standard Reference Database 17, Version 7.0 (Web Version), Release 1.4, August 2006, http://kinetics.nist.gov/kinetics
[44] A. Galano, J. R. Alvarez-Idaboy, L. A. Montero, and A. Vivier-Bunge, J. Comput. Chem. **22**, 1138 (2001).
[45] I. W. M. Smith and A. R. Ravishankara, J. Phys. Chem. A **106**, 4798 (2002).
[46] S. S. Brown, J. B. Burkholder, R. K. Talukdar, and A. R. Ravishankara, J. Phys. Chem. A **105**, 1605 (2001).
[47] E. Jimenez, T. Gierczak, H. Stark, J. B. Burkholder, and A. R. Ravishankara, J. Phys. Chem. **108**, 1139 (2004).
[48] E. R. Lovejoy, T. P. Murrells, A. R. Ravishankara, and C. J. Howard, J. Phys. Chem. **94**, 2386 (1990).
[49] G. L. Vaghjiani and A. R. Ravishankara, J. Phys. Chem. **93**, 7833 (1999).
[50] L. F. Keyser, J. Phys. Chem. **84**, 1659 (1980).
[51] R. R. Baldwin and R. W. Walker, J. Chem. Soc., Faraday Trans. 1 **75**, 140 (1979).
[52] W. Hack, K. Hoyermann, and H. G. Wagner, Proc. Symp. Chem. Kinet. Data Upper Lower Atmos. **1974**, 329 (1975).
[53] N. R. Greiner, J. Phys. Chem. **72**, 406 (1968).